INVESTIGATION OF THE EFFECT OF ROTATIONAL SPEED ON THE STATIC BENDING OF COMPOSITE BEAMS

Duong Manh Tuan[1,*]

DOI: https://doi.org/10.57001/huih5804.2026.005

ABSTRACT

Functionally graded material (FGM) are widely employed in the fields of construction, transportation, and national defense structures. Using an enhanced beam theory, this study examines the static bending response of a beam rotating about a fixed axis, in which the beam is only partially supported by an elastic foundation. The beam consists of three layers of materials: the two surface layers are made of functionally graded materials whose properties vary according to an exponential law, while the core layer is ceramic. The formulations are developed using the finite element approach without the need for any shear correction factors, highlighting the advantages of the adopted theoretical approach. After verifying the reliability of the method, the paper examines the effects of several specific parameters on the static bending response of the beam, particularly the thickness ratios of the layers, rotational speed, material composition ratio, and the distance between the axis of rotation and the beam. The findings provide significant scientific and practical insights for rotating beam-type structures.

Keywords: *Rotating, Finite element method, Static bending, FGM.*

[1]Institute of Technical Engineering, Hanoi, Vietnam
[*]Email: tuanmanhvkt123@gmail.com
Received: 10/11/2025
Revised: 20/01/2026
Accepted: 28/01/2026

1. INTRODUCTION

A novel class of composite materials, known as functionally graded materials (FGMs), is composed of two or more distinct constituents most commonly a ceramic–metal combination in which the material properties vary continuously along a specific direction. Owing to the presence of the ceramic phase, FGM-based structures exhibit excellent thermal resistance and are therefore well suited for applications under thermally influenced operating conditions. Consequently, the mechanical response of structures fabricated from these materials, particularly FGM beams, has attracted considerable attention from researchers worldwide [1-5]. In addition, in engineering practice, various components such as turbine blades, propellers for aircraft, and similar elements can be modeled as beam-like structures undergoing rotational motion. Several representative studies concerning such rotating structural systems can be cited as follows. Gunjal and Dixit [6] examined vibration mitigation in rotating beams through shape optimization, formulating the beam model using the finite element method and performing the optimization using a sequential quadratic programming approach. Pradhan and Murmu [7] investigated the mechanical response of a rotating nanobeam by adopting Eringen's nonlocal elasticity theory within a single nonlocal beam framework, with the differential quadrature method employed for the numerical analysis. Li and colleagues [8] the free-vibration characteristics of a rotating functionally graded (FGM) beam using a dynamic formulation that accounts for the coupled effects of bending and axial stretching. Amir et al. [9] analyzed the lead-lag vibration response of rotating microbeams by integrating Euler-Bernoulli and Timoshenko beam formulations with the finite element approach. Jung-Woo and Jung-Youn [10] studied the effect of cracks on the natural frequencies of a rotating Euler-Bernoulli beam using a novel numerical scheme, in which the crack-induced changes were efficiently assessed via the transfer matrix method. Das [11] employed the Ritz method, within a Timoshenko-beam framework, to investigate the in-plane and out-of-plane responses of a rotating FGM beam, while incorporating the effects of Coriolis acceleration. Xu et al. [12] investigated the dynamic response and vibration attenuation of a rotating beam under magnetic excitation, deriving the governing equations via Hamilton's principle and implementing the Galerkin method for the solution. Alireza and Cai [13] performed a

free-vibration analysis of a rotating beam within the framework of Eringen's nonlocal elasticity theory. Liang and co-workers [14] addressed vibration suppression in a rotating piezoelectric FGM beam under thermal conditions by employing a higher-order, fully coupled modeling formulation. Dejin et al. [15] introduced a combined model coupling Timoshenko beam kinematics with a modified couple stress theory to characterize the free-vibration behavior of rotating multilayer composite microbeams, including the influence of geometric imperfections.

Based on the existing studies, it can be observed that no research has yet focused on the bending responses of rotating FGM sandwich beams resting on elastic foundations. Therefore, this paper aims to investigate the static bending response of such beams by integrating the finite element approach with a newly developed beam theory. This theory is straightforward and enables the formulation of strain-stress relationships without the need for any shear correction parameters, while still accurately capturing the relevant mechanical behavior.

2. COMPUTATIONAL MODEL AND CALCULATION FORMULA

Consider a beam with the configuration shown in Fig. 1, rotating about a fixed axis with an angular velocity of Ω. The distance from the beam's tip to the axis of rotation is r_t. The beam is partially supported by an elastic foundation, characterized by two foundation parameters, k_w and k_s, with the length of the supported portion denoted as a_n. The beam has a total length L, a cross-section of height h, and width b.

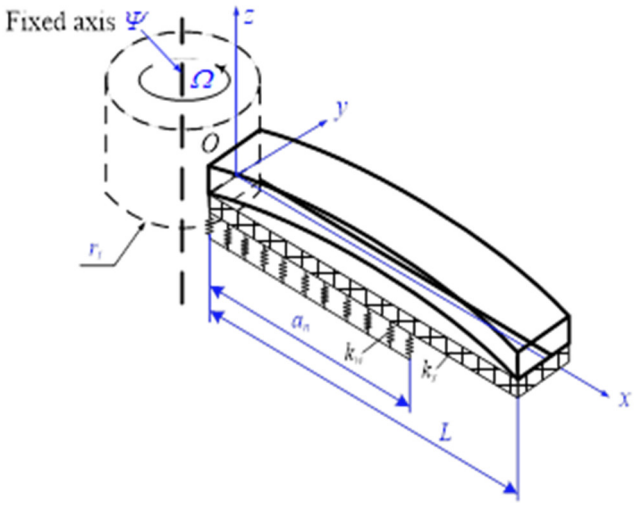

(a) Three-dimensional model

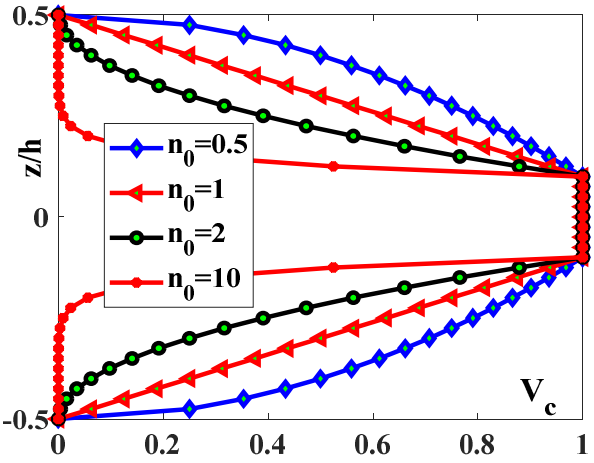

(b) The volume fraction V_c distribution along the thickness

Figure 1. A beam undergoing rotation about a fixed axis

The beam is subjected to a uniformly distributed load. To establish the governing equations, the present study employs an improved higher-order shear deformation theory, according to which the displacement field at an arbitrary point:

$$\begin{cases} u_1(x,z) = u_{01}(x,y) - z\dfrac{\partial u_{3b}}{\partial x} - k(z)\dfrac{\partial u_{3s}}{\partial x} \\ u_3(x,z) = u_{3b} + u_{3s} \end{cases} \quad (1)$$

where $k(z) = \dfrac{z}{1+\dfrac{16}{7h^2}\left(\dfrac{z^4}{h^2}+z^2\right)}$. The function $k(z)$ indicates that the beam's shear deformation is taken into account while still satisfying the boundary condition of vanishing transverse shear stresses at the beam surfaces. This represents a distinct advantage of the beam theory employing $k(z)$ over the classical beam theory and the first-order shear deformation beam theory.

Strain field of the sandwich beam:

$$\begin{aligned} \varepsilon_{xx} &= \frac{\partial u_1}{\partial x} = \frac{\partial u_{01}}{\partial x} - z\frac{\partial^2 u_{3b}}{\partial x^2} - k(z)\frac{\partial^2 u_{3s}}{\partial x^2} \\ &= \frac{\partial u_{01}}{\partial x} + z\left(-\frac{\partial^2 u_{3b}}{\partial x^2}\right) + k(z)\left(-\frac{\partial^2 u_{3s}}{\partial x^2}\right) \\ &= \varepsilon_{01} + z\varepsilon_{bx} + k(z)\varepsilon_{sx} \\ \gamma_{xz} &= \left(1-\frac{\partial k(z)}{\partial z}\right)\frac{\partial u_{3s}}{\partial x} = \left(1-\frac{\partial k(z)}{\partial z}\right)\gamma_{sxz} \end{aligned} \quad (2)$$

where:

$$\varepsilon_{01} = \frac{\partial u_{01}}{\partial x}, \varepsilon_{bx} = \left(-\frac{\partial^2 u_{3b}}{\partial x^2}\right), \varepsilon_{sx} = \left(-\frac{\partial^2 u_{3s}}{\partial x^2}\right), \gamma_{sxz} = \frac{\partial u_{3s}}{\partial x} \quad (3)$$

The normal stresses σ_{xx} corresponding to the mechanical strains, as well as the shear stresses τ_{xz}:

$$\begin{Bmatrix}\sigma_{xx}\\ \tau_{xz}\end{Bmatrix}=E(z)\begin{Bmatrix}\varepsilon_{xx}\\ \dfrac{1}{2\left(1+\nu(z)\right)}\gamma_{xz}\end{Bmatrix} \tag{4}$$

in which the beam material is specified by the following expressions [1]:

$$\begin{aligned}E^{(i)}(z)&=(E_c-E_m)\,V_c^{(i)}+E_m\\ \rho^{(i)}(z)&=(\rho_c-\rho_m)\,V_c^{(i)}+\rho_m\\ \nu^{(i)}(z)&=(\nu_c-\nu_m)\,V_c^{(i)}+\nu_m\end{aligned} \tag{5}$$

with the relationship between the ceramic and metal volume fractions given by

$$V_{\mathrm{m}}^{(i)}+V_{\mathrm{c}}^{(i)}=1 \tag{6}$$

The volumetric fraction of the ceramic can be described by various functional laws; however, the power-law formulation is the most widely used [1, 3-5]. Therefore, this work also adopts this formulation for the surface layer [1]:

$$\begin{cases}V_{\mathrm{c}}^{(1)}=\left(\dfrac{2z+h}{h-h_1}\right)^{n_0}; & -0.5h\le z\le -0.5h_1\\ V_{\mathrm{c}}^{(2)}=1; & -0.5h_1\le z\le 0.5h_1\\ V_{\mathrm{c}}^{(3)}=\left(\dfrac{2z-h}{h_1-h}\right)^{n_0}; & 0.5h_1\le z\le 0.5h\end{cases} \tag{7}$$

where n_0 is the material volume exponent, and the variation of the ceramic volume fraction in each material layer is illustrated in Fig. 1b.

Virtual work of the sandwich beam:

$$\begin{aligned}\delta\Pi^{beam}&=\int_V\left(\delta\sigma_{xx}^T\varepsilon_{xx}+\delta\tau_{xz}^T\gamma_{xz}\right)dV\\ &=\int_V\left(\delta\begin{Bmatrix}\varepsilon_{01} & z\varepsilon_{bx} & k(z)\varepsilon_{sx}\end{Bmatrix}^T E\begin{Bmatrix}\varepsilon_{01}\\ z\varepsilon_{bx}\\ k(z)\varepsilon_{sx}\end{Bmatrix}\right)dV\\ &+\int_V\left(\delta\left\{\frac{\partial k(z)}{\partial z}\gamma_{sxz}\right\}^T\frac{E(z)}{2\left(1+\nu(z)\right)}\left\{\frac{\partial k(z)}{\partial z}\gamma_{sxz}\right\}\right)dV\\ &=\int_V\begin{pmatrix}\delta\varepsilon_{01}^TE(z)\varepsilon_{01}+\delta\varepsilon_{01}^TzE(z)\varepsilon_{bx}+\delta\varepsilon_{01}^Tk(z)E(z)\varepsilon_{sx}\\ \delta\varepsilon_{bx}^TE(z)z\varepsilon_{01}+\delta\varepsilon_{bx}^TE(z)z^2\varepsilon_{bx}+\delta\varepsilon_{bx}^TE(z)zk(z)\varepsilon_{sx}\\ \delta\varepsilon_{sx}^TE(z)k(z)\varepsilon_{0x}+\delta\varepsilon_{sx}^TE(z)zk(z)\varepsilon_{bx}+\delta\varepsilon_{sx}^TE(z)k^2(z)\varepsilon_{sx}\end{pmatrix}dV\\ &+\int_V\left(\left(1-\frac{\partial k(z)}{\partial z}\right)^2\frac{E(z)}{2\left(1+\nu(z)\right)}\delta\gamma_{sxz}^T\gamma_{sxz}\right)dV\end{aligned} \tag{8}$$

Virtual work of the forces interacting with the elastic foundation:

$$\delta\Pi^{found}=b\int_L\begin{pmatrix}k_w\delta\left(u_{3b}+u_{3s}\right)\left(u_{3b}+u_{3s}\right)\\ +k_s\left(\delta\dfrac{\partial\left(\left(u_{3b}+u_{3s}\right)\right)}{\partial x}\right)\dfrac{\partial\left(\left(u_{3b}+u_{3s}\right)\right)}{\partial x}\end{pmatrix}dx \tag{9}$$

where k_w and k_s represent the two foundation stiffness parameters.

For a beam undergoing rotation, the work of the inertial forces generated by the rotational motion on the beam can be expressed as [15]:

$$\delta\Pi^{ro}=\int_L\left(F_\omega(x)\left(\delta\frac{\partial\left(u_{3b}+u_{3s}\right)}{\partial x}\right)\frac{\partial\left(u_{3b}+u_{3s}\right)}{\partial x}\right)dx \tag{10}$$

where the centrifugal force F_ω is given by [15]:

$$F_\omega=\frac{1}{2}\int_L\sum_{i=1}^{3}\int_{h_i}^{h_{i+1}}\left(\rho(z)\omega^2\left[r(L-x)+\frac{1}{2}\left(L^2-x^2\right)\right]\right)dzdx \tag{11}$$

At this stage, the work performed by the external load on the beam is expressed as follows:

$$\delta\Pi^{forced}=b\int_L\left(u_{3b}^T+u_{3s}^T\right)\mathbf{P}_0dx \tag{12}$$

In order to obtain the equilibrium equations, the principle of virtual work is applied to the FGM beam:

$$\delta\Pi^{forced}-\delta\Pi^{beam}-\delta\Pi^{found}-\delta\Pi^{ro}=0 \tag{13}$$

For the analysis, a two-node beam element is employed, with four degrees of freedom assigned to each node:

$$\mathbf{u}_e=\sum_{i=1}^{2}\begin{Bmatrix}u_{01i}\\ u_{3bi}\\ u_{3si}\\ \left(\dfrac{\partial u_{3b}}{\partial x}\right)_i\\ \left(\dfrac{\partial u_{3s}}{\partial x}\right)_i\end{Bmatrix} \tag{14}$$

And, in this case, the Lagrange (N_i) and Hermite (H_i) interpolation functions for the displacement components take the following forms

$$\begin{cases}u_{01}=\sum_{i=1}^{2}N_iu_{01i}=\boldsymbol{N}_u\boldsymbol{u}_e\\ u_{3b}=\sum_{i=1}^{2}\left\{H_iu_{3bi}+H_{i+1}\left(\dfrac{\partial u_{3b}}{\partial x}\right)_i\right\}=\boldsymbol{H}_b\boldsymbol{u}_e\\ u_{3s}=\sum_{i=1}^{2}\left\{H_iu_{3si}+H_{i+1}\left(\dfrac{\partial u_{3s}}{\partial x}\right)_i\right\}=\boldsymbol{H}_s\boldsymbol{u}_e\\ \dfrac{\partial u_{3b}}{\partial x}=\sum_{i=1}^{2}\left\{\dfrac{\partial H_i}{\partial x}u_{3bi}+\dfrac{\partial H_{i+1}}{\partial x}\left(\dfrac{\partial u_{3b}}{\partial x}\right)_i\right\}=\boldsymbol{H}_{bx}\boldsymbol{u}_e\\ \dfrac{\partial u_{3s}}{\partial x}=\sum_{i=1}^{2}\left\{\dfrac{\partial H_i}{\partial x}u_{3si}+\dfrac{\partial H_{i+1}}{\partial x}\left(\dfrac{\partial u_{3s}}{\partial x}\right)_i\right\}=\boldsymbol{H}_{sx}\boldsymbol{u}_e\\ \dfrac{\partial^2u_{3b}}{\partial x^2}=\sum_{i=1}^{2}\left\{\dfrac{\partial^2H_i}{\partial x^2}u_{3bi}+\dfrac{\partial^2H_{i+1}}{\partial x^2}\left(\dfrac{\partial u_{3b}}{\partial x}\right)_i\right\}=\boldsymbol{H}_{b2x}\boldsymbol{u}_e\\ \dfrac{\partial^2u_{3s}}{\partial x^2}=\sum_{i=1}^{2}\left\{\dfrac{\partial^2H_i}{\partial x^2}u_{3si}+\dfrac{\partial^2H_{i+1}}{\partial x^2}\left(\dfrac{\partial u_{3s}}{\partial x}\right)_i\right\}=\boldsymbol{H}_{s2x}\boldsymbol{u}_e\end{cases} \tag{15}$$

And:

$$\boldsymbol{u}=\begin{Bmatrix} u_{01} \\ u_{3b} \\ u_{3s} \\ \left(\dfrac{\partial u_{3b}}{\partial x}\right) \\ \left(\dfrac{\partial u_{3s}}{\partial x}\right) \end{Bmatrix}=\begin{bmatrix} \boldsymbol{N}_u \\ \boldsymbol{H}_b \\ \boldsymbol{H}_s \\ \boldsymbol{H}_{bx} \\ \boldsymbol{H}_{sx} \end{bmatrix}\boldsymbol{u}_e=\boldsymbol{H}\boldsymbol{u}_e \tag{16}$$

Strain components are evaluated in terms of the nodal displacements as:

$$\begin{cases} \varepsilon_{01}=\dfrac{\partial u_{01}}{\partial x}=\dfrac{\partial \mathrm{N}_u}{\partial x}\boldsymbol{u}_e=\boldsymbol{B}_u\boldsymbol{u}_e \\ \varepsilon_{bx}=-\dfrac{\partial^2 u_{3b}}{\partial x^2}=-\boldsymbol{H}_{b2x}\boldsymbol{u}_e=\boldsymbol{B}_b\boldsymbol{u}_e \\ \varepsilon_{sx}=-\dfrac{\partial^2 u_{3s}}{\partial x^2}=-\boldsymbol{H}_{s2x}\boldsymbol{u}_e=\boldsymbol{B}_s\boldsymbol{u}_e \end{cases}; \tag{17}$$

$$\gamma_{sxz}=\frac{\partial u_{3s}}{\partial x}=\boldsymbol{H}_{sx}\boldsymbol{u}_e$$

The expression for the work done of the beam element is given by:

$$\begin{aligned} \delta\Pi_e^{beam}&=\delta\boldsymbol{u}_e^T\int_V\begin{pmatrix} \boldsymbol{B}_u^TE\boldsymbol{B}_u+\boldsymbol{B}_u^TzE\boldsymbol{B}_b+\boldsymbol{B}_u^Tk(z)E\boldsymbol{B}_s \\ \boldsymbol{B}_b^TEz\boldsymbol{B}_u+\boldsymbol{B}_b^TEz^2\boldsymbol{B}_b+\boldsymbol{B}_b^TEzk(z)\boldsymbol{B}_s \\ \boldsymbol{B}_s^TEk(z)\boldsymbol{B}_u+\boldsymbol{B}_s^TEzk(z)\boldsymbol{B}_b+\boldsymbol{B}_s^TEk^2(z)\boldsymbol{B}_s \end{pmatrix}dV\boldsymbol{u}_e \\ &+\delta\boldsymbol{u}_e^T\int_V\left(\left(1-\frac{\partial k(z)}{\partial z}\right)^2\frac{E}{2(1+\nu)}\boldsymbol{H}_{sx}^T\boldsymbol{H}_{sx}\right)dV\boldsymbol{u}_e \\ &=\delta\boldsymbol{u}_e^T\boldsymbol{K}_e^{beam}\boldsymbol{u}_e \end{aligned} \tag{18}$$

where the stiffness matrix of the beam element has the form:

$$\boldsymbol{K}_e^{beam}=\int_V\begin{pmatrix} \boldsymbol{B}_u^TE\boldsymbol{B}_u+\boldsymbol{B}_u^TzE\boldsymbol{B}_b+\boldsymbol{B}_u^Tf(z)E\boldsymbol{B}_s \\ \boldsymbol{B}_b^TEz\boldsymbol{B}_u+\boldsymbol{B}_b^TEz^2\boldsymbol{B}_b+\boldsymbol{B}_b^TEzf(z)\boldsymbol{B}_s \\ \boldsymbol{B}_s^TEf(z)\boldsymbol{B}_u+\boldsymbol{B}_s^TEzf(z)\boldsymbol{B}_b+\boldsymbol{B}_s^TEf^2(z)\boldsymbol{B}_s \\ +\left(1-\dfrac{\partial k(z)}{\partial z}\right)^2\dfrac{E}{2(1+\nu)}\boldsymbol{H}_{sx}^T\boldsymbol{H}_{sx} \end{pmatrix}dV \tag{19}$$

The computation of the beam element stiffness matrix as given in Eq. (19) does not require reduced integration or any shear correction factor. This is because the contribution of shear deformation is fully represented, thereby preventing shear locking, unlike in the Timoshenko beam theory. This feature also constitutes an advantage of the shear-deformation theory expressed in Eq. (1).

The work done of the centrifugal inertial force and the elastic foundation can be expressed as:

$$\begin{aligned} \delta\Pi_e^{found}&=\delta\boldsymbol{u}_e^T\left(b\int_L\begin{pmatrix} k_w\left(\boldsymbol{H}_b+\boldsymbol{H}_s\right)^T\left(\boldsymbol{H}_b+\boldsymbol{H}_s\right) \\ +k_s\left(\boldsymbol{H}_{bx}+\boldsymbol{H}_{sx}\right)^T\left(\boldsymbol{H}_{bx}+\boldsymbol{H}_{sx}\right) \end{pmatrix}dx\right)\boldsymbol{u}_e \\ &=\delta\boldsymbol{u}_e^T\boldsymbol{K}_e^{found}\boldsymbol{u}_e \\ \delta\Pi_e^{ro}&=\delta\boldsymbol{u}_e\left(\int_L\left\{F_\omega(x)\left(\boldsymbol{H}_{bx}+\boldsymbol{H}_{sx}\right)^T\left(\boldsymbol{H}_{bx}+\boldsymbol{H}_{sx}\right)\right\}dx\right)\boldsymbol{u}_e \\ &=\delta\boldsymbol{u}_e^T\boldsymbol{K}_e^{ro}\boldsymbol{u}_e \end{aligned} \tag{20}$$

The work of the external forces:

$$\delta\Pi^{forced}=\delta\boldsymbol{u}_e^T\left(b.\int_L\left(\boldsymbol{H}_b+\boldsymbol{H}_s\right)\boldsymbol{P}_0dx\right)=\boldsymbol{u}_e^T\boldsymbol{P}_e \tag{21}$$

Inserting expressions (15) - (17) into equation (10) yields the static equilibrium equation of the beam rotating about a fixed axis as:

$$\sum_e\left(\boldsymbol{K}_e^{beam}+\boldsymbol{K}_e^{found}+\boldsymbol{K}_e^{ro}\right)\boldsymbol{u}_e=\sum_e\boldsymbol{P}_e \tag{22}$$

By solving equation (22), the displacements of the bending beam are obtained. Modifications in foundation characteristics, rotation speed, or the distance r_t to the axis of rotation alter the stiffness matrices on the left-hand side, thereby affecting the beam's response.

3. VERIFICATION STUDY

This example investigates the bending behavior of a simply supported (S-S) beam. L =16h, E = 70GPa, ν = 0.3. The beam is loaded by a uniformly distributed transverse load denoted as P_0, The deflection at the midspan of the beam is evaluated according to the following formula $u^*=\dfrac{384EI_0}{5P_0L^4}u_{3\max}$ (with $I_0 = bh^3/12$). Table 1 presents the midspan deflections obtained in the present study and those derived from the Ritz approach [16], in which an incrementally refined mesh is employed in this example. The computational results indicate that a 12-element mesh provides the required accuracy. Accordingly, this mesh configuration is adopted for the subsequent analyses.

Table 1. The convergence of the solution and the comparison of the midspan deflection of the beam subjected to a uniformly load, L = 16h, S-S (* elements)

Present					Ritz approach [16]
8*	9*	10*	12*	14*	
1.0094	1.0094	1.0094	1.0094	1.0094	1.0097

The beam is simply supported at both ends and rests on an elastic foundation characterized by two stiffness coefficients. The beam has a length L and a cross-section of thickness h, with the foundation's stiffness parameters denoted as $K_w^{\wedge} = \frac{k_w L^4}{EI}$ and $K_s^{\wedge} = \frac{k_s L^2}{EI}$ (with $I = bh^3/12$). The beam is loaded by a uniformly distributed transverse load with a magnitude of P_0. Table 2 presents the midspan deflections $u_3^* = \frac{EI}{P_0 L^4} u_{3\max}$ obtained in the present study, alongside those computed using the Differential Quadrature Method (DQM) [17] and the exact solutions [18].

Table 2. Comparison of the midspan deflections for a beam subjected to a uniformly distributed load and for a beam, L = 120h, S-S

Foundation parameters		Midspan deflections		
$K_w^{\wedge}$	$K_s^{\wedge}$	DQM [17]	Exact [18]	Present
0	0	1.302290	1.3033	1.301692
	10	0.644827	0.6457	0.644679
	25	0.366111	0.3671	0.366063
10	0	1.180567	1.1814	1.180075
	10	0.613325	0.6141	0.613192
	25	0.355668	0.3566	0.355622
100	0	0.640074	0.6403	0.639927
	10	0.425582	0.4261	0.425517
	25	0.282846	0.2836	0.282817

4. NUMERICAL RESULTS AND THEIR DISCUSSION

This section presents the computational results for the bending deflection of a sandwich beam rotating about a fixed axis. The thickness ratios of the layers are denoted as 2-1-2, 1-1-1, 1-2-1, and 1-8-1. For the 2-1-2 configuration, this notation indicates that the two surface layers have equal thicknesses and that each surface layer is twice as thick as the core layer; the other notations are interpreted in the same manner.

The nondimensional parameters are defined as follows:

$$R_w = 100\frac{E_c h^3}{P_0 L^4} u_{3\max};\ K_w^* = \frac{k_w L^4}{T_0};$$
$$K_s^* = \frac{k_s L^2}{T_0};\ \Omega^* = L^2\omega\sqrt{\frac{12\rho}{E_m h^2}};\ T_0 = \frac{E_c h^3}{12} \quad (23)$$

Figs. 2, 3 illustrate the variation of the beam deflection as the thickness ratios of the layers change. These results indicate that:

- As the core thickness increases, the beam becomes stiffer due to the higher proportion of ceramic material, which in turn leads to a reduction in the beam's deflection.

- For a simply supported beam, due to the combined effects of the elastic foundation and rotational speed, the maximum deflection does not occur at the midspan. Instead, the location of the maximum deflection shifts toward the right.

- For a cantilever beam with one fixed end and one free end, the maximum deflection occurs at the free end. Moreover, as the distance from the beam axis to the rotation axis increases, the maximum deflection of the beam decreases.

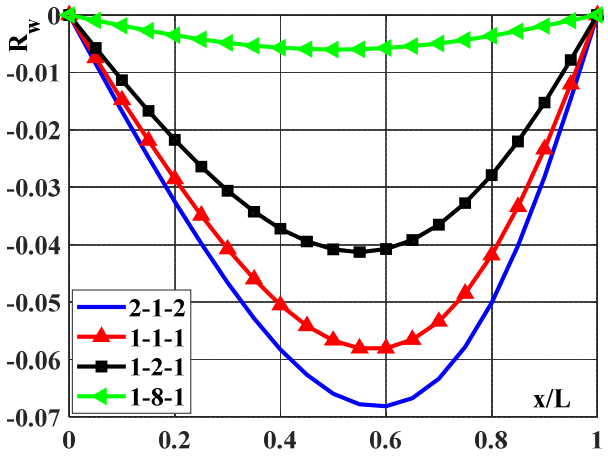

(a) $r_t/L = 0.5$

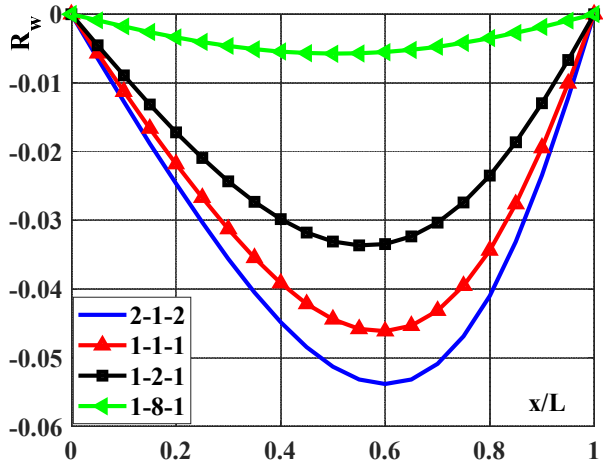

(b) $r_t/L = 1$

Figure 2. The variation of the deflection with respect to the layer thickness ratios is analyzed for a beam simply supported at both ends, S-S, $K_w^{\wedge} = 300$, $K_s^* = 30, \Omega^* = 20, a_n/L = 0.25$

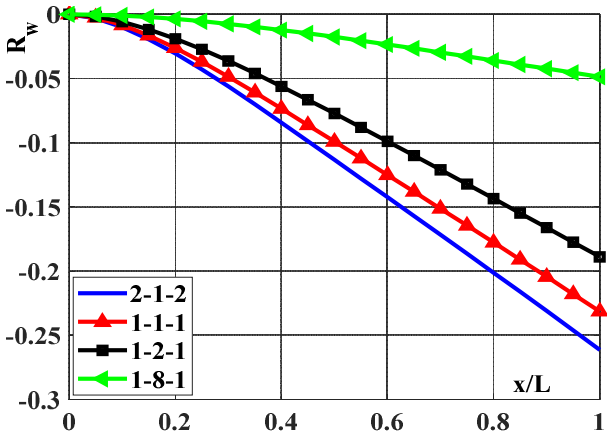

(a) $r_t/L = 0.5$

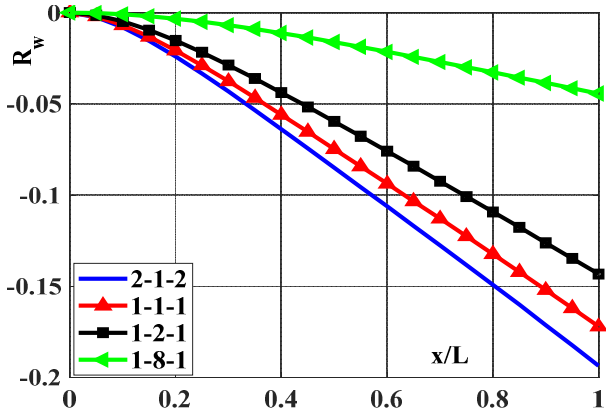

(b) $r_t/L = 1$

Figure 3. Dependence of the beam deflection on the layer thickness ratios, C-F, $K_w^{\wedge} = 300$, $K_s^* = 30$, $\Omega^* = 20$, $a_n/L = 0.25$

The distance from the rotation axis to the beam, denoted as r_t, is varied from 0 to 2L. The computed deflection profiles along the beam are presented in Fig. 4. The results show that increasing r_t leads to a reduction in the beam's maximum deflection. The maximum deflection of the clamped–clamped (C-C) beam is significantly smaller than that of the simply supported (S-S) beam. Moreover, the influence of the distance r_t is more pronounced for the S–S beam than for the C-C beam.

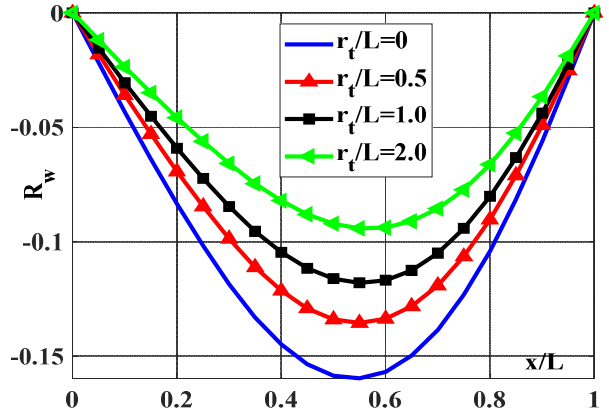

(a) SS

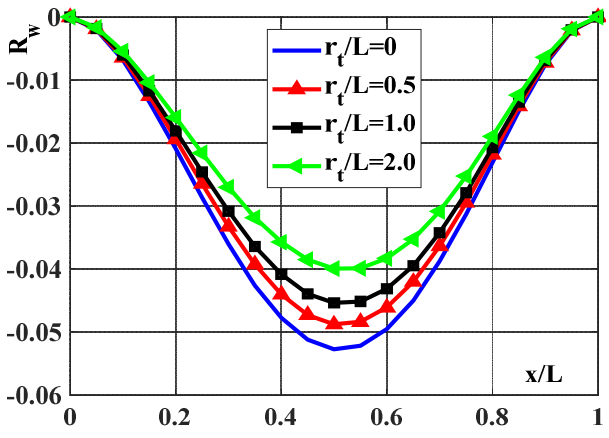

(b) CC

Figure 4. Dependence of beam deflection on the distance between the rotation axis and the beam, $\Omega^* = 10$, $a_n/L = 0.25$, $n_0 = 2$, $K_w^{\wedge} = 300$, $K_s^* = 30$, 2-1-2

The power-law exponent of the volume fraction, denoted as n_0, is gradually increased from 0 to 5. The resulting beam deflections are plotted in Fig. 5. These findings indicate that:

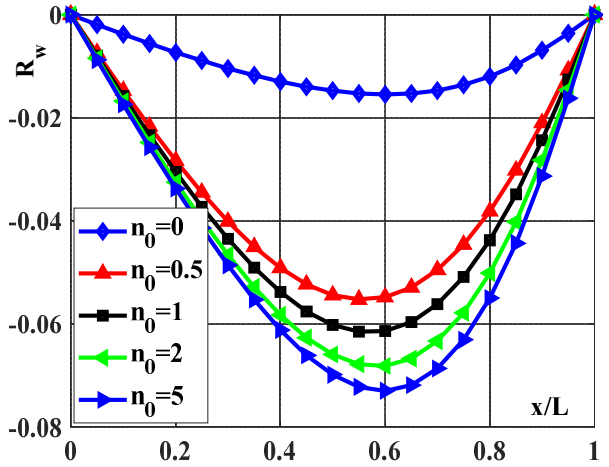

(a) S-S

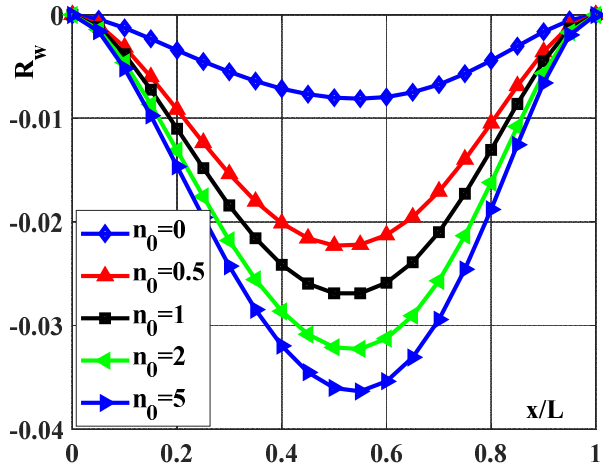

(b) C-C

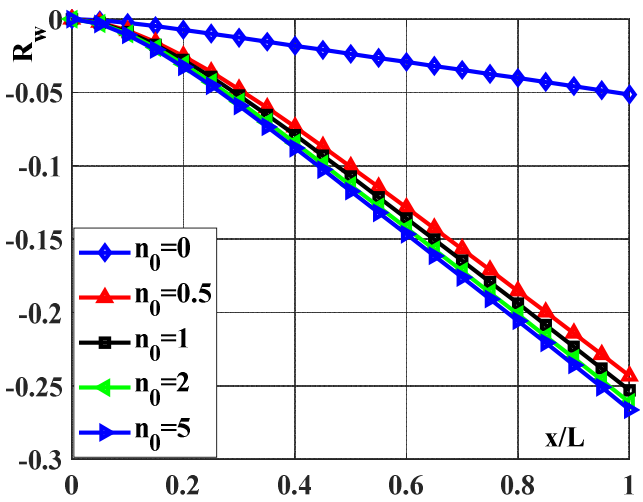

(c) C-F

Figure 5. Dependence of the beam deflection on the material volume fraction exponent, $\Omega^* = 20$, $a_n/L = 0.25$, $K_w^\wedge = 300$, $K_s^* = 30$, 2-1-2, $r_t/L = 0.5$

- As the material volume fraction exponent increases, the maximum deflection of the beam also increases. This is due to the higher proportion of metal within the beam, which makes the beam more flexible.

- When the material volume fraction exponent n_0 varies from 0 to 0.5, the beam deflection exhibits the most significant change. For n_0 values greater than 0.5, the deflection of the sandwich beam changes only slightly. Simultaneously, owing to the influence of inertial forces induced by the rotational motion, the beam's deflection profile tends to shift toward the right-hand side.

The rotational speed of the beam is gradually increased so that the value of Ω^* varies from 0 to 25. The resulting deflection profiles of the beam are plotted in Fig. 6. Several observations can be drawn from these results as follows:

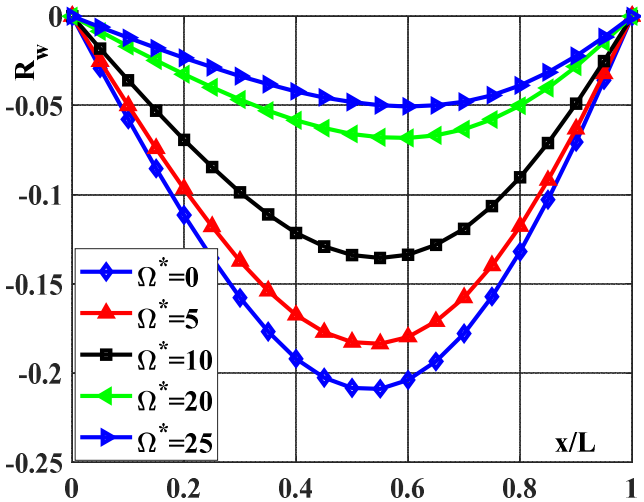

(a) S-S

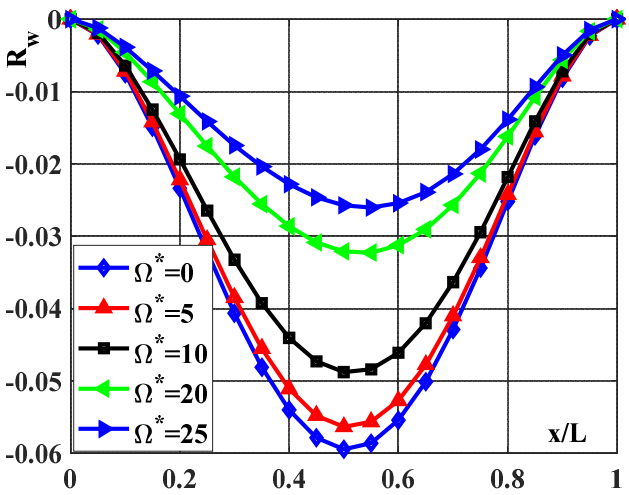

(b) C-C

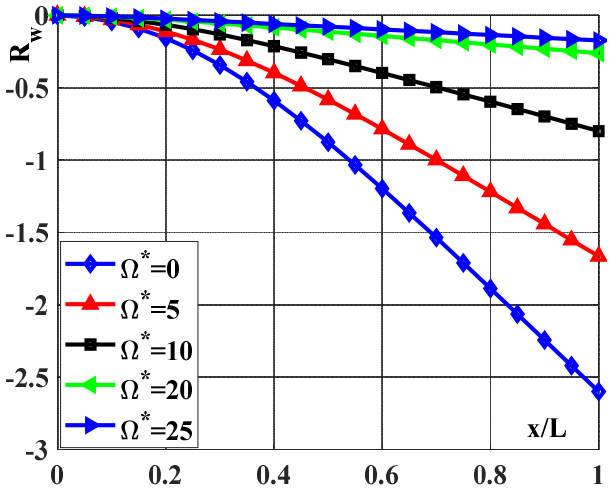

(c) C-F

Figure 6. Dependence of the beam deflection on the rotational speed Ω^*, $n_0 = 2$, $a_n/L = 0.25$, $K_w^\wedge = 300$, $K_s^* = 30$, 2-1-2, $r_t/L = 0.5$

- As the rotational speed increases, the beam's maximum deflection decreases, indicating that centrifugal inertial effects play a significant role in the response of the rotating beam.

- For beams with symmetric boundary conditions (simply supported at both ends or clamped at both ends), the rotational speed affects both the deflection profile and the location of the maximum deflection, while also influencing the magnitude of the maximum deflection.

5. CONCLUSION

This paper presented a finite element method combined with a refined shear deformation theory to analyze the static bending response of sandwich beams partially resting on an elastic foundation and rotating about a fixed axis. The proposed computational approach has been reliably validated through comparisons with

previously published results. The study also investigated the effects of several parameters, including foundation stiffness, rotational speed, material composition ratios, and the distance from the beam to the rotation axis, yielding scientifically and practically significant findings. Based on the results of this research, the design and application of multilayer rotating composite beams with functionally graded materials should consider multiple factors, with particular attention to the beam's rotational speed and the distance from the beam end to the rotation axis.

REFERENCES

[1]. Reddy JN., "Free vibration analysis of functionally graded ceramic-metal plates, Analysis and Design of Plated Structures," *Anal Design Plated Struct*, 1, 293-321, 2007.

[2]. Ning Z., Tahir K., Haomin G., Shaoshuai S., Wei Z., Weiwei Z., "Functionally Graded Materials: An Overview of Stability, Buckling, and Free Vibration Analysis," *Adv Mat Science Engi,* 1354150, 2019.

[3]. Thom DV., Duc DH., Minh PV., Tung NS., "Finite element modelling for free vibration response of cracked stiffened FGM plates," *Vietnam J Science Techn,* I58 (1), 119-129, 2020.

[4]. Hoai VN., Doan DH., Khoa NM., Thom VD., Tran HT., "Phase-field buckling analysis of cracked stiffened functionally graded plates," *Comp Struct,* 217, 50-59, 2019.

[5]. Nguyen HN., Tan TC., Luat DT., Phan VD., Thom DV., Minh PV., "Research on the Buckling Behavior of Functionally Graded Plates with Stiffeners Based on the Third-Order Shear Deformation Theory," *Materials,* 12 (8), 1262, 2019.

[6]. Gunjal SK., Dixit US., "Vibration analysis of shape-optimized rotating cantilever beams," *Eng. Optimiz,* 39 (1), 105-123, 2007.

[7]. Pradhan SC., Murmu T., "Application of nonlocal elasticity and DQM in the flapwise bending vibration of a rotating nanocantilever," *Physica E: Low-dimens Systems Nanostr,* 42, 1944–1949, 2010.

[8]. Li L., Zhang DG., Zhu WD., "Free vibration analysis of a rotating hub–functionally graded material beam system with the dynamic stiffening effect," *J. Sound Vibr,* 333, 1526–1541, 2014.

[9]. Amir MDS., Mehdi BJ., Dehrouyeh M., "On size-dependent lead-lag vibration of rotating microcantilevers," *Int J Eng Science,* 101, 50-63, 2016.

[10]. Jung-Woo L., Jung-Youn L., "In-plane bending vibration analysis of a rotating beam with multiple edge cracks by using the transfer matrix method," *Meccanica,* 52, 1143-1157, 2017.

[11]. Das D., "Free vibration and buckling analyses of geometrically non-linear and shear-deformable FGM beam fixed to the inside of a rotating rim," *Compos Struct,* 179, 628-645, 2017.

[12]. Xu X., Han Q., Chu F., "Vibration suppression of a rotating cantilever beam under magnetic excitations by applying the magnetostrictive material," *J Intell Mater Syst Struct*, 30(4), 576-592, 2019.

[13]. Alireza B., Cai X.Y., "Vibration analysis of rotating rods based on the nonlocal elasticity theory and coupled displacement field," *Microsyst Technol*, 25, 1077-1085, 2019.

[14]. Liang L., Wei-Hsin L., Dingguo Z., Yang Z., "Vibration control and analysis of a rotating flexible FGM beam with a lumped mass in temperature field," *Compos Struct*, 208, 244-260, 2019.

[15]. Dejin C., Kai F., Shijie Z., "Flapwise vibration analysis of rotating composite laminated Timoshenko microbeams with geometric imperfection based on a re-modified couple stress theory and isogeometric analysis," *Eur J Mech A/Solids*, 76, 25-35, 2019.

[16]. Simsek M., "Static analysis of a functionally graded beam under a uniformly distributed load by Ritz method," *Int J Eng Appl Sci,* 1(3), 1-11, 2009.

[17]. Chen W.Q., Lu C.F., Bian Z.G., "A mixed method for bending and free vibration of beams resting on a Pasternak elastic foundation," *Appl Math Model*, 28, 877-890, 2004.

[18]. Wang C.M., Lam K.Y., He X.Q., "Exact solutions for Timoshenko beams on elastic foundations using Green's functions," *Mech Struct Mach,* 26(1), 101-113, 1998.